JOURNAL OF Applied Polymer SCIENCE

Electrospun Nanofibers from a Multihole Spinneret with Uniform Electric Field

Yuansheng Zheng,[1] Xuekai Liu,[1] Yongchun Zeng[1,2]

[1]Department of Textile Engineering, College of Textiles, Donghua University, Songjiang, Shanghai 201620, People's Republic of China

[2]Key Laboratory of Textile Science & Technology (Donghua University), Ministry of Education, Shanghai 201620, People's Republic of China

Correspondence to: Y. Zeng (E-mail: yongchun@dhu.edu.cn).

ABSTRACT: This study presents a multihole spinneret with a metal flat electrode to obtain uniform electric field and meet a high production requirement. We demonstrate that the multihole spinneret produces finer fiber diameters and more concentrated fiber mat compared to the conventional multineedle electrospinnig system. This study focuses on the effect of the electric field distribution on the spinning process and the resultant nanofibers. The three-dimensional electric field simulation results show that the multihole spinneret creates not only a more uniform electric field, but also a stronger electric field except for the area very close to the spinneret. The measurement of the electric field verifies the simulation results. This study shows that fine fibers, as well as concentrated and thick fiber mat can be obtained by this multihole electrospinning system at a high production rate. © 2013 Wiley Periodicals, Inc. J. Appl. Polym. Sci. 130: 3221–3228, 2013

KEYWORDS: electrospinning; fibers; molding

Received 26 December 2012; accepted 15 May 2013; Published online 14 June 2013

DOI: 10.1002/app.39553

INTRODUCTION

Nanofibrous nonwovens are a kind of nonwoven products manufactured with the nanofibers of diameter below 1 μm. Nonwoven structure has unique features, including interconnected pores and a very large surface-to-volume ratio, which enables such nanofibrous nonwovens to have many applications in areas of filtration media, life science, medicine, and industry.[1,2] Electrospinning and melt blowing are the most commonly used processes for producing nanofibrous nonwovens. Melt-blowing technique has already been in wide commercial use. However, the melt-blown fibers are usually still on submicroscale. On the other hand, despite the fact that electrospinning can produce nanofibers that have diameters in the 100 nm range, widespread industrial implementation of electrospun nanofibers is primarily limited by low production rate, which is typically 0.01–1 g/h from a single capillary. Therefore, mass production of nanofibers by electrospinning still creates great interest for the researchers.

Several methods have been developed to increase the electrospinning productivity. These previously reported approaches are generally classified as multineedle and needleless electrospinning. This kind of classification may lead to some misunderstanding in the case of a spinneret with holes instead of needles be used for electrospinning.[3–5] Thoppey et al.[6] have classified the approaches to scale-up electrospinning based on the manner in which the polymer solution is dispensed, as using either a confined or unconfined fluid-volume feed method. Confined systems contain the spinneret with needles,[6–8] holes,[3–5] and microfluidic channels[9] to eject the polymer solution. In this article, we refer to these processes as "multineedle electrospinning" though sometimes holes are used to take the replace of needles. In a multineedle electrospinning system, the solution is injected at a constrained rate. Conversely, in unconfined feed systems, a polymer solution flows unconstrained over a free liquid surface.[10–14] We refer to the unconfined feed method as "needleless electrospinning," although it is described as "free surface electrospinning" by Forward and Rutledge.[15]

Although much more configurations of needleless setups have been reported than those of multineedle setups, multineedle electrospinning is still under active investigation. Multineedle electrospinning is a simple way to scale-up the productivity. Moreover, due to the confined feed method of a multineedle system, the restricted flow rate is important for maintaining a continuous stable electrospinning process, controlling the collection of the fiber mats, and controlling the fiber diameters. In multineedle systems, the polymer solution is injected into enclosed capillaries such as needles or holes. Therefore, special structure fibers such as core–shell nanofibers can be produced with multineedle systems.

The major disadvantage in multineedle systems is nonuniform electric field on each needle tip of the spinneret, which leads to processing problems such as clogging. Moreover, the repulsive electric fields between the needles produced by the multiple point charges will lead to jet repulsion and collecting difficulty, and consequently result in a nonuniform mat. To stabilize the electrospinning process and control fiber repulsion in multineedle systems, auxiliary or secondary electrodes have been used to modify the electric field distribution. Kim et al.[16] added a cylindrical electrode in the multineedle eletrospinning process to stabilized the spun jet, Yang et al.[17] used a coaxial shield ring to create an apporximate uniform electric field near the tips of the needles and to restrict the collection area, and Alessio et al[18] employed a secondary electrode to reduce the divergence angle between jets. In all these cases the fiber repulsion was effectively controlled. Researchers have noted that electric field influences the multineedle electrospinning process and the fiber morphology. Angammana and Jayaram[19] investigated the variation of the strength of the electric field at the tip of the needles in multineedle arrangements and showed that the local field deterioration at the needle tips degraded the electrospinning process significantly and produced considerable variation in the morphology of the fiber.

In the previous work,[20] we have used an auxiliary plate to achieve more uniform electric field in a three-needle system. The needles have been inserted into and protruded from the holes on the plate. The effect of the needle length protruding from the plate has been investigated. The results show that the reduced needle length produces smaller fiber diameters. The smallest fiber diameters are obtained when the needle length is as small as 0, which indicates that the needles are removed and a uniform electric field with a flat spinneret is formed. Starting from this knowledge, in this study, a spinneret comprised of a plastic plate with drilled holes and a metal cylindrical electrode is used to replace the spinneret with needles. The purpose is to design a uniform electric field to produce finer fibers with narrower fiber distribution and more uniform fiber mat at a higher production rate. The use of holes not only reduces the complexity and cost of manufacturing, but also creates a more uniform electric field in the absence of needles.

Electrospun nanofibers have been produced from holes (or pores) on a tube[3,4] or on a flat surface[5] to increase the flow rate of electrospinning. Unfortunately, electric field analysis has not been taken into account in their research. In this work, a seven-hole spinneret is used for scale-up the production rate of electrospun nanofibers. Experimental work is carried out to compare the electrospinning process and fiber morphology of the new design and the conventional seven-needle system. We find that the seven-hole system produced finer fibers and more concentrated fiber mat. Three-dimensional (3D) electric fields of both the seven-hole and seven-needle systems are simulated to understand the effects of electric field distribution on electrospinning performance.

EXPERIMENTS AND SIMULATION

Material Preparation

Polyethylene oxide (PEO, M_v = 600 000 g/mol, Sigma-Aldrich, Missouri) was used as received. PEO powder was dissolved in distilled water into solution with 5.0 wt % concentration, and the solution was prepared at the ambient temperature.

Experimental Setup

The schematic of the seven-hole electrospinning setup is shown in Figure 1(a). In this work the plastic plate with 5-mm thickness made of polytetrafluoroethylene (PTFE) was used for creating the electrospinning jets due to its hydrophobic and dielectric characters. Seven 0.5-mm holes were drilled on the PTFE surface, with a 10 mm spacing between neighboring holes, as shown in Figure 1(b). The holes on PTFE surface were equilateral hexagon distributed as shown in Figure 1(c), since equilateral hexagon structure was the best one to maximize the total amount of jets per unit area.[17] The polymer solution was forced from a syringe via a syringe pump (KDS 220, KD Scientific, Massachusetts) through a 2 mm inner diameter silicone rubber tube to a 2 mm outer diameter metallic tube inlet to provide solution feeding. The inlet tube was inserted in the center of the metal cylindrical electrode with a diameter of 5 cm, and the solution was charged prior to reaching the plastic surface. A solution chamber was formed between the electrode and plastic plate. A high voltage power supply with operating voltage ranging from 0 to 40 kV and resolution of 0.1 kV was applied to the spinneret and the collector. An aluminum foil-grounded collector was employed to collect the electrospun fibers.

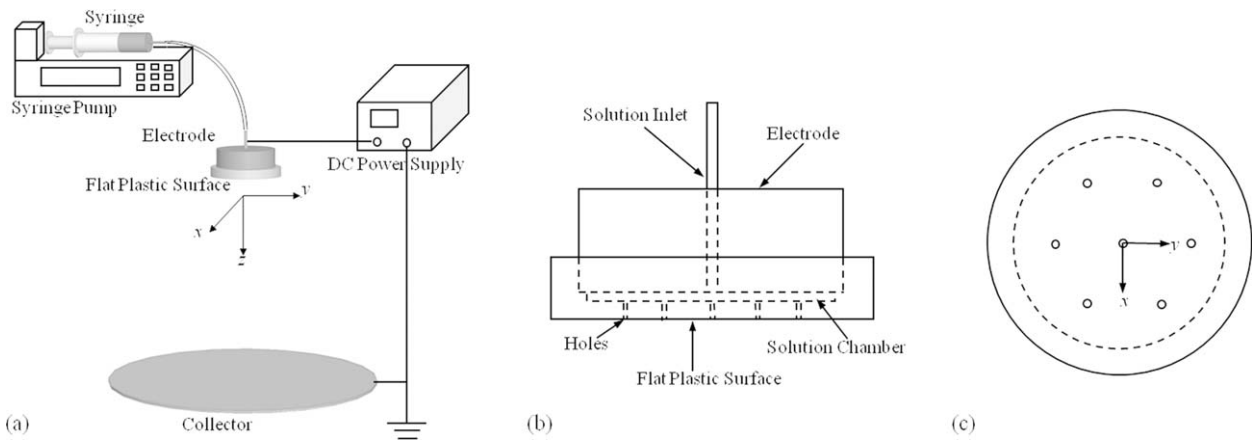

Figure 1. (a) Schematics of experimental setups; (b) sectional view of the spinneret; (c) arrangement of the holes.

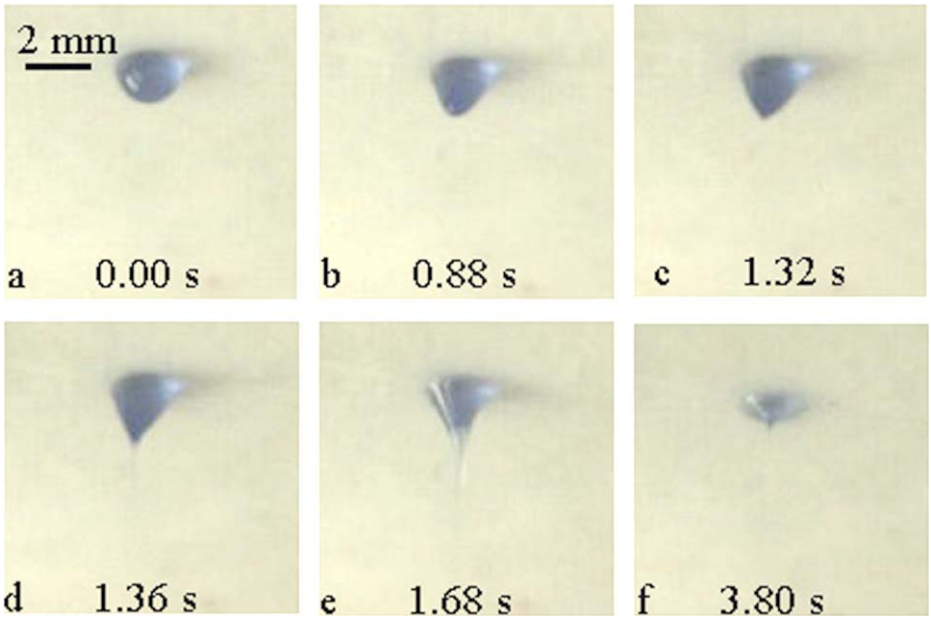

Figure 2. The subsequent jet initiation process. [Color figure can be viewed in the online issue, which is available at wileyonlinelibrary.com.]

Experiments for a conventional seven-needle setup were also done as a reference. The stainless steel needle was blunt-tip type with an outer diameter of 0.8 mm, inner diameter of 0.5 mm, and length of 36 mm. The needle array was identical with the hole array for the seven-hole spinneret.

Characterization

The electrospun fibers were observed with a scanning electron microscope (SEM) (JSM-5600LV, Japan). Each sample was sputtercoated with gold for analysis. Five SEM images taken from different sample locations were used to measure the fiber diameters. The mean diameter of the fibers was calculated using 300 measurements randomly selected. Image J software (NIH, Maryland) was used to determine the fiber diameters.

Electric Field Simulation

The 3D electric fields were simulated by Ansoft Maxwell (ANSYS) software using the finite element method (FEM) with electrostatic solution type. All the electric field strength, E, were calculated. Before the simulation, the physical geometries of the electrospinning setups (e.g., spinneret and collector), polymer solution in the chamber and needles were established according to their practical dimensions, locations, and relative permittivities. The computation domain is axsymmetric. High voltage was set to the electrode and the needles as the excitations, and the aluminum collector and the boundaries at an infinite distance were set as zero potential. The meshing and solving were performed by the software to obtain the electric field intensity and profile.

RESULTS AND DISCUSSION

Jet Initiation

The shape of the polymer droplet at the needle tip during a single-needle electrospinning process has been described by Kong et al..[21] In this study, the jet formation process from a hole was captured with high-speed photography. A Redlake HG-100K

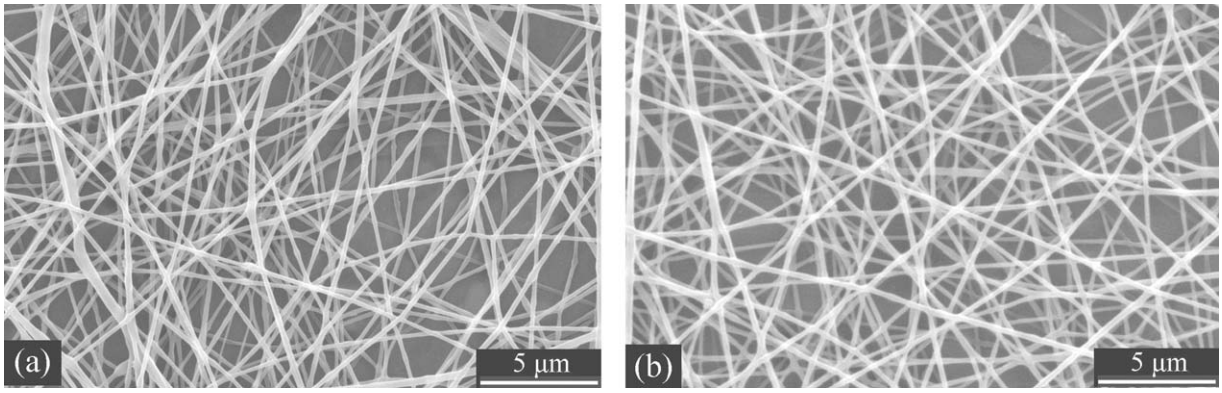

Figure 3. SEM images of PEO fibers produced by (a) seven-hole system and (b) seven-needle system. The processing parameters are: applied voltage 25 kV, working distance 25 cm, and flow rate 3.5 mL/h.

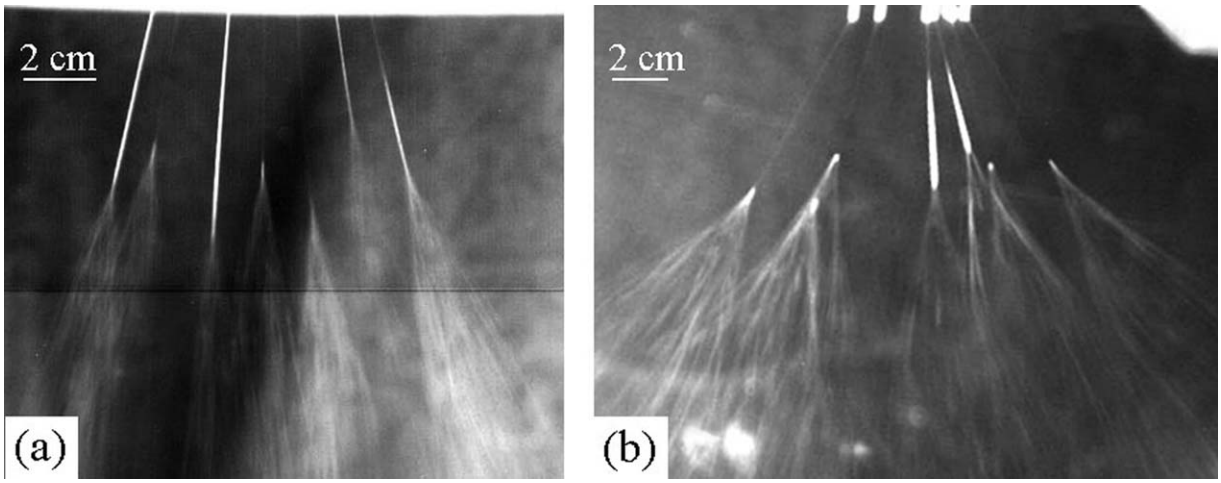

Figure 4. Photographs taken at long exposure times (33.33 ms) of the electro-spinning processes of (a) seven-hole system and (b) seven-needle system.

high-speed camera (Redlake, San Diego) was used. This camera has the capability of recording images at a frame rate of 1000 frames/s or up to 10,0000 partial frames/s. Full frames are recorded at a resolution of 1504 × 1128 pixels. The camera was equipped with a Nikon 24–85 mm, f 2.8 zoom lens. The light source was two 1300 W lamps. Image processing and analysis was done with Adobe Photoshop and the software supplied with the camera.

A typical jet formation sequence is shown in Figure 2. The PEO polymer solution is tinted with a commercial dye (0.001 wt %) to improve the imaging contrast. At time zero, the PEO solution is suspended by surface tension and viscoelastic stresses at the orifice in the form of a hole on the PTFE surface [Figure 2(a)]. The electrical potential is applied for a little more than 0.88 s earlier. The droplet is transformed into a conical shape by the applied electric potential [Figure 2(b)]. The rounded tip becomes sharper [Figure 2(c)] and a jet emanates from the tip of the cone [Figure 2(d)]. The shape of the cone changes into a small size, for the rapidly elongating and thinning jet flowed from the droplet [Figure 2(e)]. The shape of the cone is stable and persists as long as the solution is fed by the pump after about 2 s [Figure 2(f)].

The resultant PEO fibers produced by the new designed seven-hole electrospinning system are shown in Figure 3(a), and the obtained fiber diameters are around 150 nm. Also shown is the morphology of the fibers produced by the conventional seven-needle system [Figure 3(b)]. The fibers have a uniform cylindrical morphology with few bead defects present.

Comparison of Seven-Hole and Seven-Needle Electrospinning Systems

Experimental Results. The electrospinning processes of seven-hole and seven-needle systems were photographed with a long exposure time, shown in Figure 4. It can be seen that the seven-hole electrospinning system obtains lower jets divergence degree

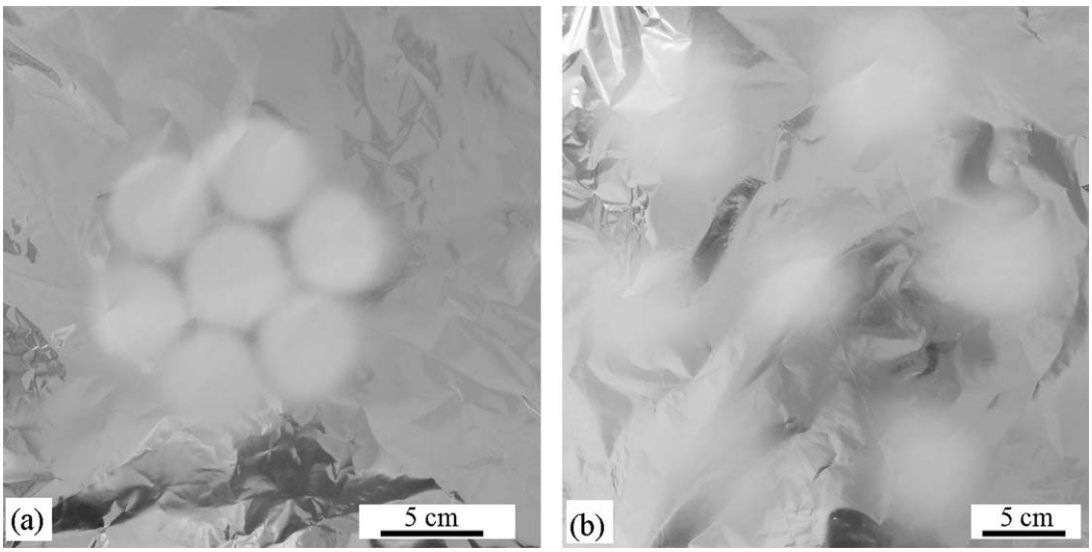

Figure 5. Fiber mats collected from (a) seven-hole system and (b) seven-needle system. The collecting time is 3 min. The processing parameters are: applied voltage 25 kV, working distance 25 cm, and flow rate 3.5 mL/h.

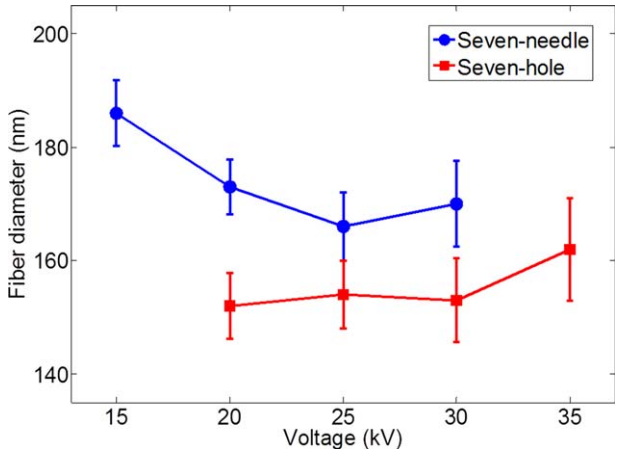

Figure 6. Fiber diameters produced by seven-hole system and seven-needle system. The processing parameters are: working distance 25 cm, and flow rate 3.5 mL/h. The length of the error bar represents one-fifth of the standard deviations of the fiber diameter. [Color figure can be viewed in the online issue, which is available at wileyonlinelibrary.com.]

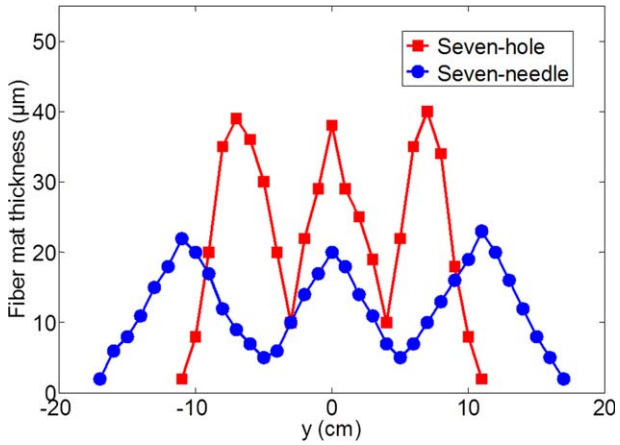

Figure 7. The thicknesses of the fiber mat collected from seven-hole system and seven-needle system. The collecting time is 60 min. The processing parameters are: applied voltage 30 kV, working distance 25 cm, and flow rate 3.5 mL/h. [Color figure can be viewed in the online issue, which is available at wileyonlinelibrary.com.]

and smaller jets whipping amplitude than those in the seven-needle system, which results in more concentrated and smaller fiber mats shown in Figure 5. It is obvious that the deposit area from each hole is almost of identical size in the seven-hole system. In contrary, for the seven-needle system, the deposit area from the central needle is smaller than that from side needles, which indicates that the side jets influence the central jet evidently. The fiber diameters and distributions of the two systems are shown in Figure 6. It can be observed that under the same processing conditions, the seven-hole system produces a smaller diameter of fibers than the seven-needle system. The standard deviations of the fiber from the seven-hole system is higher than that from seven-needle system, that maybe caused by the bigger Taylor cone of the seven-hole system, which probably produce some coarse fiber at the beginning of the spinning process. Figure 7 shows the thicknesses of the fiber mat obtained from the two systems after 60 min. The thickness was measured every 1 cm along the centre line of fiber mats. It is evident that the seven-hole system produces a much thicker fiber mat.

Simulation Results and Analysis. Figure 8 shows the electric field distributions calculated by using FEM analysis. The simulation voltage for the two systems was set to 30 kV. The arrows indicate the direction of the electric field, and their length is proportional to the strength at that position. It can be seen that the new designed seven-hole system has a more uniform electric field.

Electric field intensity distributions for the two systems are compared. Figure 9(a,b) show the electric field intensity, E, along y axis at different distances from the spinneret. For the seven-hole system [Figure 9(a)], $y = 0$ is the position of the

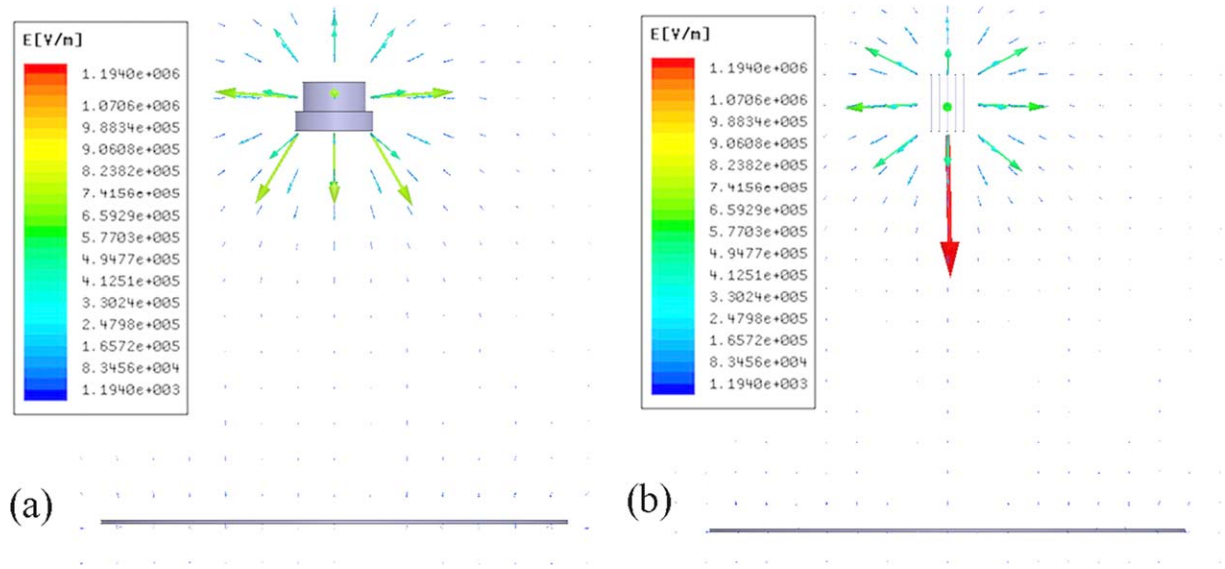

Figure 8. The electric field distribution of the two systems: (a) seven-hole system, (b) seven-needle system. [Color figure can be viewed in the online issue, which is available at wileyonlinelibrary.com.]

Applied Polymer SCIENCE

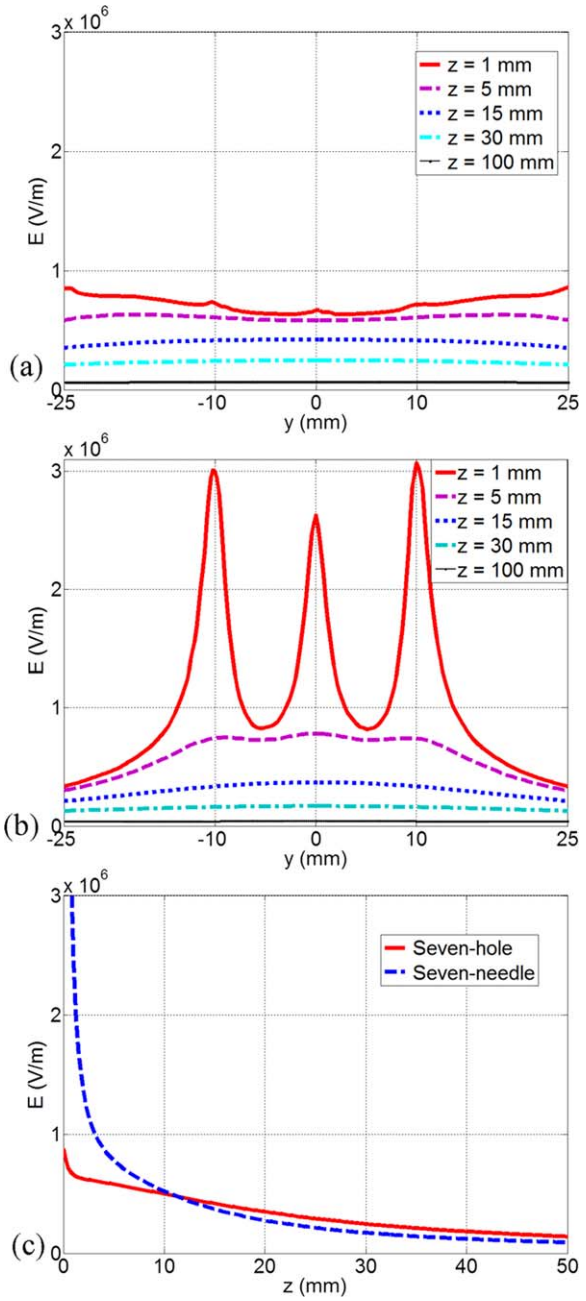

Figure 9. Comparison of the electric field intensity distributions for the two systems: (a) E distribution along y axis for seven-hole system, (b) E distribution along y axis for seven-needle system, and (c) E distribution along z axis for the two systems at central hole (needle). [Color figure can be viewed in the online issue, which is available at wileyonlinelibrary.com.]

central hole, while $y = \pm 10$ mm are the positions of two side holes [Figure 1(c)]. The same case is applied to the seven-needle system [Figure 9(b)]. The E values of the six side holes (or needles) are identical due to axisymmetric distribution of equilateral hexagon. In the area very close to the spinneret (i.e., $z = 1$ mm), intensified electric field can be found at the hole and needle positions. It can be seen that this intensified effect of the electric field is much less in the seven-hole system, which indicates that the seven-hole system produces a much uniform electric field intensity distribution near the spinneret. It is noted that for the seven-hole system, the highest electric field intensity is concentrated at the edge of the spinneret ($y = \pm 25$ mm). From Figure 9(a,b), it can be observed that although the seven-needle system produces larger E in the area close to the spinneret (i.e., $z = 1$ mm), the seven-hole system creates a more uniform electric field beyond the distance of $z = 5$ mm. This phenomenon is further confirmed by Figure 9(c), which shows the electric field intensity along z-axis of the two systems. There is a sharp decrease of electric field intensity from the spinneret to the collector for the seven-needle system but a gradual decrease for the seven-hole system. In the position of about $z = 10$ mm, E value for the seven-hole system starts to exceed that for the seven-needle system, which means that the seven-hole system creates a higher and more uniform electric field distribution except for the area very near the spinneret. In our previous study,[20] we observed that whipping occurs after the jet travels a straight path of around 5 cm. Therefore the jets in the seven-hole system undergo stronger drawing force when whipping. It is known that, whipping is the main factor responsible for the reduction of fiber diameter in the electrospinning process. The spinning jet in the seven-hole system was sufficiently stretched according to the stronger drawing force caused by the higher electric field intensity. That is the reason why the seven-hole system produces finer fibers.

To explain the concentration effect of the seven-hole system, a parameter f is defined to describe the deviation of the electric field. It is calculated as

$$f = \frac{\sqrt{E_x^2 + E_y^2}}{|E_2|} \tag{1}$$

where E_x, E_y, and E_z are the components of the electric field strength E along x, y and z axis at the side hole (needle) position, respectively, as shown in Figure 10(a). f is the tangent of the included angle α of the spinning direction and E. Figure 10(b) shows the comparison of f along the spinning direction for the two systems. The lower value of f for the seven-hole system indicates higher convergence of the electric field to the spinning line. Consequently, the new designed seven-hole system produces a more concentrated mat (Figure 5).

Electric Field Measurement Verification. To verify the electric field simulation, the electric fields of the single-hole and the single-needle electrospinning systems were measured. The electric field was measured along spinning direction (z-direction) and the direction perpendicular to the spinning line (y-direction) with EST 102 Vibration Capacitive Electrometer (ESD, China). The applied voltages for measurements were set as 2 kV for the two systems. The measurements started from the position of 3 mm away from the spinneret, for the probe was easily broken when it was too close to the charged spinneret. Meanwhile, electric field simulation under the conditions in accordance with the experimental parameters was carried out.

Figure 11(a) shows the comparison of the simulation results and measured values of the centerline voltages along z-axis, and Figure 11(b) compares the simulation and measured voltages along y-axis at the distance of $z = 5$ mm for the two systems. The simulation

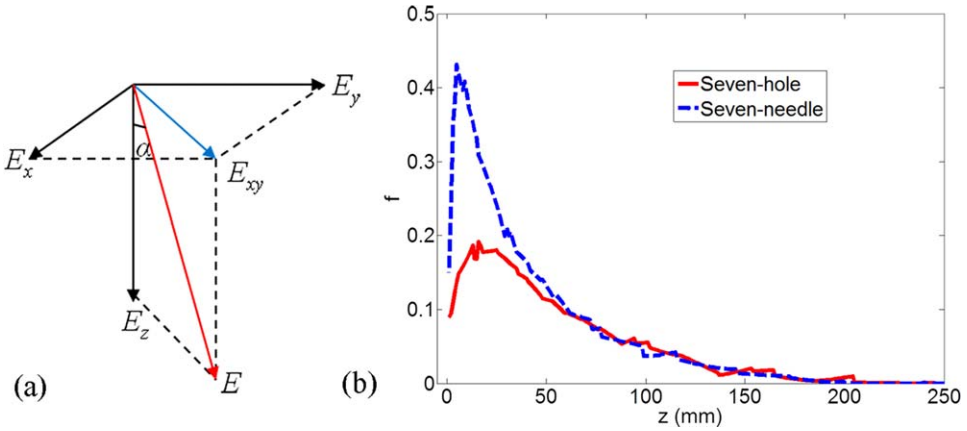

Figure 10. (a) Illustration of α and (b) calculated *f* for the two electrospinning systems. [Color figure can be viewed in the online issue, which is available at wileyonlinelibrary.com.]

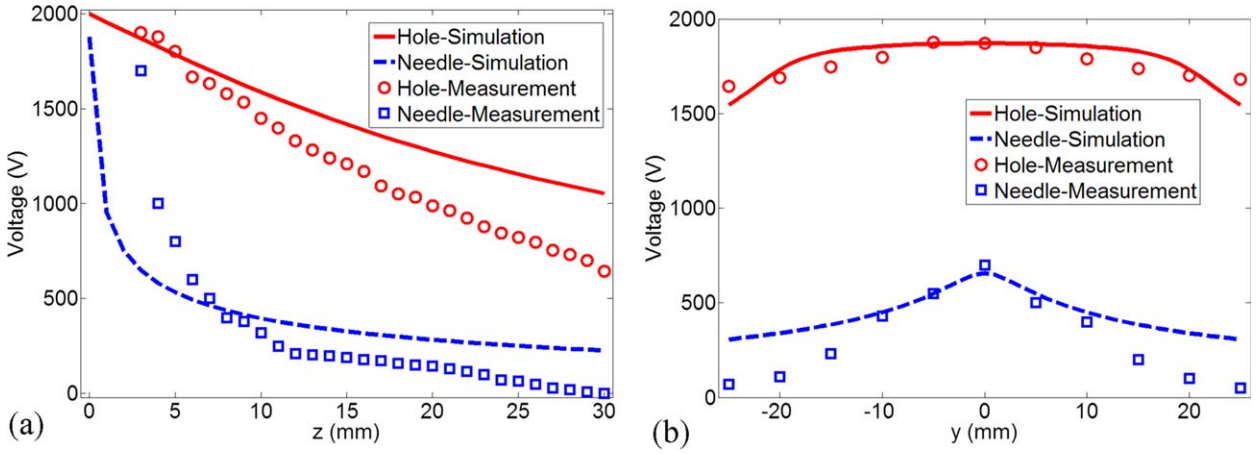

Figure 11. Comparison of simulation results and measured values of voltage: (a) the centerline along *z*-axis, and (b) along *y*-axis at distance of $z = 5$ mm. [Color figure can be viewed in the online issue, which is available at wileyonlinelibrary.com.]

and measurement results are shown to be in good agreement. The single-hole system produces a more uniform electric field. Beyond the distance of $z = 5$ mm, the voltage under the single-hole spinneret is higher than that of the single-needle spinneret.

Scale-Up Analysis

The productivity of the electrospinning setup is determined as the weight of the nanofibrous mat collected for a certain time interval. The weighting of nanofibrous mats was carried out on a laboratory electronic balance after 1 h spinning. The productivities of the two systems were investigated under the respective applied voltages as shown in Figure 12, and the productivity of conventional single needle setup under the same electrospinning process (0.5 mL/h flow rate and 25 cm working distance) was carried out as comparisons. The productivities of the two systems are increased with the increasing applied voltage. When the operating voltage increases, the stronger electric field leads to more solution ejected from the spinneret. For the seven-needle system, the central needle cannot form a jet when the

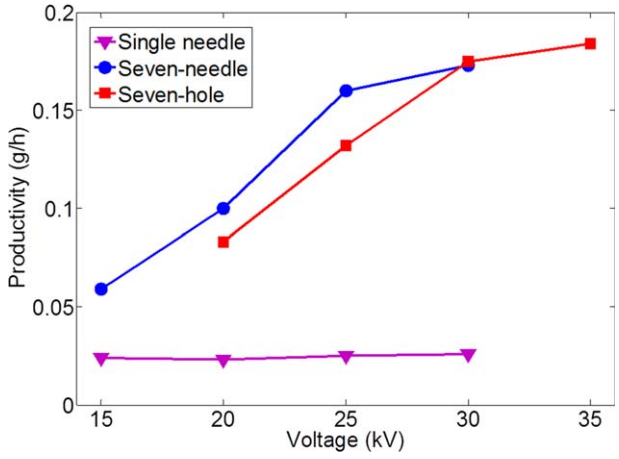

Figure 12. Effect of applied voltage on fiber productivity. [Color figure can be viewed in the online issue, which is available at wileyonlinelibrary.com.]

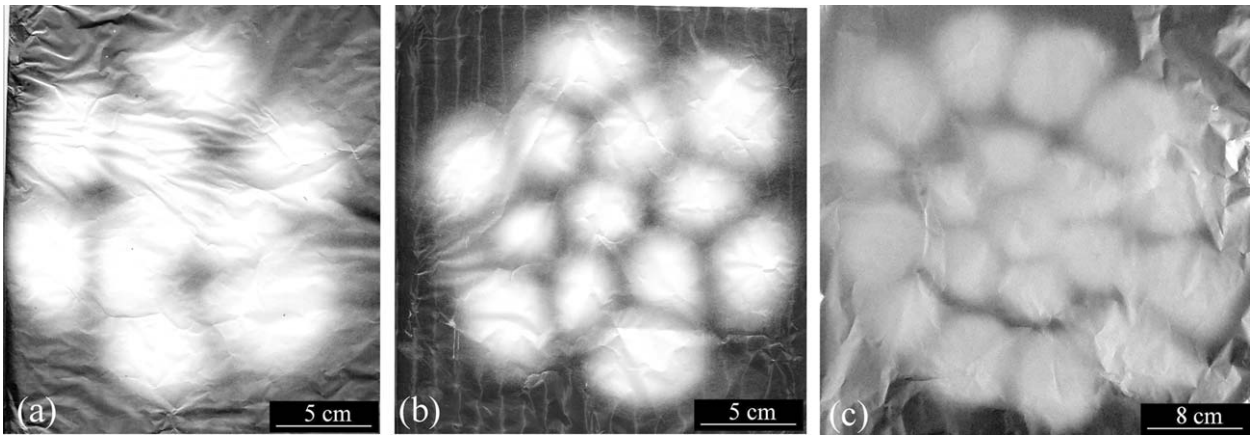

Figure 13. Fiber mats produce by multineedle system with various numbers of holes on the spinneret: (a) 10 holes (30 kV, 25 cm working distance, 5 mL/h flow rate), (b) 13 holes (32 kV, 25 cm working distance, 6.5 mL/h flow rate) and (c) 19 holes (40 kV, 25 cm working distance, 9.5 mL/h flow rate).

applied voltage is less than 15 kV, and this phenomenon also appears in the central hole of the seven-hole system at 20 kV. The productivity of the seven-needle and seven-hole system is about seven times that of the single-needle setup, which is about 0.025 g/h under the 30 kV applied voltage, and the productivity of the seven-hole system is a little higher than that of the seven-needle system beyond 30 kV. Figures 13 show the collected fiber mats produced by the multihole electrospinning setups with different hole numbers. Using the new designed multihole electrospinning setup, the rate of electrospinning can be scaled-up by increasing the hole number and the circle number of the hole distribution.

CONCLUSIONS

In this work, we demonstrate a new multihole electrospining configuration with a flat electrode. We compare a seven-hole electrospinning system with a conventional seven-needle system to study the effect of electric field distribution on spinning. The experimental and simulation results show that the multihole system creates a more uniform electric field, and the electric field under the multihole spinneret is stronger except for the area very close to the spinneret. Consequently, finer fibers are obtained from the multihole system. A parameter f is introduced to describe the convergence of the electric field distribution. It is shown that the multihole system has a smaller f, and therefore produces more concentrated and thicker fiber mat. The measurement of the electric field verifies the simulation results. The multihole system can produce nanofibers at a mass rate higher than that can be achieved in the single needle setup, and the throughput can be easily scaled-up by increasing the hole number on the spinneret.

ACKNOWLEDGMENTS

This work was financially supported by the National Natural Science Foundation of China (11272088), Shanghai Dawning Program (10SG33), and the Fundamental Research Funds for the Central Universities.

REFERENCES

1. Zhang, Y.; Chwee, T. L.; Ramakrishna, S.; Huang, Z. M. *J. Mater. Sci.: Mater. Med.* **2005**, *16*, 933.
2. Burger, C.; Hsiao, B. S.; Chu, B. *Annu. Rev. Mater. Res.* **2006**, *36*, 333.
3. Dosunmu, O. O.; Chase, G. G.; Kataphinan, W.; Reneker, D. H. *Nanotechnology* **2006**, *17*, 1123.
4. Varabhas, J. S.; Chase, G. G.; Reneker, D. H. *Polymer* **2008**, *49*, 4226.
5. Zhou, F. L.; Gong, R. H.; Isaac, P. *J. Mater. Sci.* **2009**, *44*, 5501.
6. Thoppey, N. M.; Bochinski, J. R.; Laura, I. C.; Russell, E. G. *Polymer* **2010**, *51*, 4928.
7. Theron, S.; Yarin, A. L.; Zussman, E.; Kroll, E. *Polymer* **2005**, *46*, 2889.
8. Alessio, V.; Fabio, R.; Giorgio, M.; Claudio, T.; Renato, C. *Polym. Int.* **2010**, *59*, 1606.
9. Srivastava, Y.; Loscertales, I.; Marquez, M.; Thorsen, T. *Microfluid. Nanofluid.* **2008**, *4*, 245.
10. Niu, H. T.; Lin, T.; Wang, X. G. *Polym. Eng. Sci.* **2009**, *114*, 3524.
11. He, J. H.; Liu, Y. *Chaos Soliton. Fract.* **2008**, *37*, 643.
12. Yarin, A. L.; Zussman, E. *Polymer* **2004**, *45*, 2977.
13. Wang, X.; Niu, H. T.; Lin, T. *Polym. Eng. Sci.* **2009**, *49*, 1582.
14. Thoppey, N. M.; Bochinski, J. R.; Clarke, L. I.; Gorga, R. E. *Nanotechnology* **2011**, *22*, 345301.
15. Forward, K. M.; Rutledge, G. C. *Chem. Eng. J.* **2012**, *183*, 492.
16. Kim, G.; Cho, Y. S.; Kim, W. D. *Eur. Polym. J.* **2006**, *42*, 2031.
17. Yang, Y.; Jia, Z. D.; Hou, L.; Liu, J. N.; Wang, L. M.; Guan, Z. C. *IEEE Trans. Dieletr. Electr. Insul.* **2010**, *17*, 1592.
18. Alessio, V.; Riccardo, A.; Giorgio, M. *J. Mater. Process. Technol.* **2009**, *209*, 5178.
19. Angammana, C. J.; Jayaran, S. H. *IEEE Trans. Ind. Appl.* **2011**, *47*, 1028.
20. Xie, S.; Zeng, Y. C. *Ind. Eng. Chem. Res.* **2012**, *51*, 5336.
21. Kong, C. S.; Lee, T. H.; Kim, H. S. *J. Mater. Sci.* **2007**, *42*, 8016.